ADVANCES IN ATMOSPHERIC SCIENCES, VOL. 29, NO. 3, 2012, 544–560

Low-Frequency Coupled Atmosphere–Ocean Variability in the Southern Indian Ocean

FENG Junqiao*[1,2] (冯俊乔), HU Dunxin[1,2] (胡敦欣), and YU Lejiang[3] (于乐江)

[1] *Institute of Oceanology, Chinese Academy of Sciences, Qingdao* 266071

[2] *Key Laboratory of Ocean Circulation and Waves, Chinese Academy of Sciences, Qingdao* 266071

[3] *Applied Hydrometeorological Research Institute, Nanjing University of Information Science and Technology, Nanjing* 210044

(Received 27 June 2011; revised 28 November 2011)

ABSTRACT

The low-frequency atmosphere–ocean coupled variability of the southern Indian Ocean (SIO) was investigated using observation data over 1958–2010. These data were obtained from ECMWF for sea level pressure (SLP) and wind, from NCEP/NCAR for heat fluxes, and from the Hadley Center for SST. To obtain the coupled air-sea variability, we performed SVD analyses on SST and SLP. The primary coupled mode represents 43% of the total square covariance and is featured by weak westerly winds along 45°–30°S. This weakened subtropical anticyclone forces fluctuations in a well-known subtropical dipole structure in the SST via wind-induced processes. The SST changes in response to atmosphere forcing and is predictable with a lead-time of 1–2 months. Atmosphere–ocean coupling of this mode is strongest during the austral summer. Its principle component is characterized by mixed interannual and interdecadal fluctuations. There is a strong relationship between the first mode and Antarctic Oscillation (AAO). The AAO can influence the coupled processes in the SIO by modulating the subtropical high. The second mode, accounting for 30% of the total square covariance, represents a 25-year period interdecadal oscillation in the strength of the subtropical anticyclone that is accompanied by fluctuations of a monopole structure in the SST along the 35°–25°S band. It is caused by subsidence of the atmosphere. The present study also shows that physical processes of both local thermodynamic and ocean circulation in the SIO have a crucial role in the formation of the atmosphere–ocean covariability.

Key words: southern Indian Ocean, SST, SLP, Antarctic Oscillation

Citation: Feng, J. Q., D. X. Hu, and L. J. Yu, 2012: Low-frequency coupled atmosphere–ocean variability in the southern Indian Ocean. *Adv. Atmos. Sci.*, **29**(3), 544–560, doi: 10.1007/s00376-011-1096-2.

1. Introduction

Natural climate variability of low-frequency time scales from interannual to decadal has been the focus of numerous studies. These climate variations are believed to arise from atmosphere–ocean interactions. The dynamics of both systems are thus coupled via exchange processes at their common interface. Coupled variability of the system occurs when the atmosphere responds to forcing from the ocean and when the ocean responds to forcing from the atmosphere. To understand and determine the mechanisms governing these climatic variations, it is vital to study the common variability of both the ocean and the overlying atmospheric systems and to characterize the large-scale interactions between them. While a vast number of studies have been devoted to SST and sea level pressure (SLP) fluctuations and their coupled variability over the northern Atlantic and the northern Pacific Oceans (e.g., Deser and Blackmon, 1993; Kushnir, 1994; Latif and Barnett, 1996; Mann and Park, 1996), the Southern Hemisphere has received little attention, except for a few studies on the southern Atlantic (e.g., Venegas et al., 1997, 1998; Sterl and Hazeleger, 2003; Fauchereau et al., 2003). Related research on the southern Indian Ocean has been rare (Allan et al., 1995; Reason, 1999;

*Corresponding author: FENG Junqiao, fengjunqiao@qdio.ac.cn

Reason, 2001; Fauchereau et al., 2003). However, the southern Indian Ocean is bounded by the Antarctic circumpolar current to the south and receives oceanic water mass transport or throughflow from the Pacific Ocean via the Indonesia throughflow. The location, shape, and topography of the subcontinent make SST highly sensitive to circulation changes in the Indian Ocean (Fauchereau et al., 2003). The southern Indian Ocean not only plays an important role in the surrounding climate of continents like Africa (Reason and Godfred-Spenning, 1998), but it is also a main region where the Asian monsoon water originates. Moreover, the study by Liu et al. (2006) showed that the Indian Ocean Dipole (IOD) in the tropical Indian Ocean responds to the southern high latitude climate almost instantaneously, suggesting that the IOD signal exists in the Southern Hemisphere. Nan et al (2009) pointed out that the Indian Ocean SST has an important bridging role in the Antarctic Oscillation (AAO)–East Asian Summer Monsoon relationship. Therefore, atmosphere–ocean interaction in the southern Indian Ocean may have implications for other areas, especially the northern Indian Ocean and Asia.

Most studies on Indian Ocean variability have only considered the tropical area north of 30°S. If the southern boundary of the domain is situated farther south, additional SST anomalies in the southern Indian Ocean emerge in a subtropical dipole mode, which is phase-locked to the austral summer (Behera and Yamagata, 2001; Reason, 2001; Reason, 2002). Huang and Shukla (2007) also discussed a subtropical dipole mode in the southern Indian Ocean; however, that study still emphasized the tropical region. As is generally known, the ex-tropical southern Indian Ocean is dominated by the lower tropospheric subtropical high. It is quite likely that atmospheric forcing has a crucial role in the evolution of the subtropical dipole (Hermes and Reason, 2005). Previous studies have shown that this SST anomaly pattern is correlated with rainfall in various regions of southern Africa (e.g., Rocha and Simmonds, 1997a, b; Goddard and Graham, 1999; Reason, 1999; Reason and Mulenga, 1999; Behera and Yamagata, 2001). Surface heat flux, especially the latent heat variability, is strongly implicated in forming these SST anomalies (Behera and Yamagata, 2001; Suzuki et al., 2004; Hermes and Reason, 2005; Huang and Shukla, 2008). It has been suggested that modulations of the subtropical atmospheric anticyclone are responsible for this latent heat flux variability, although the link between atmospheric variability and SST variability has not been precisely determined. Although the formation mechanism of the subtropical SST anomalies is different from that in the tropics, the SST anomalies may also be ultimately driven by coupled atmosphere–ocean interaction. Concerning decadal variability, Allan et al. (1995) presented the long-term fluctuations in the mean state of the climate system over the Indian Ocean during austral summertime, showing the strengthening and weakening of oceanic and atmospheric variables on the multidecadal time scale. However, the interactions and feedback mechanisms between the evolving SST and atmosphere–ocean circulations are not well understood. Knowledge of temporal and spatial covariability between ocean and atmosphere in the southern Indian Ocean remains inadequate.

In this study, we aimed to develop a preliminary insight into how the southern Indian Ocean system varies. Our first aim was to identify the principal modes of the SST and the overlying atmospheric circulation, providing insight into the variability of the southern Indian Ocean coupled atmosphere–ocean system on low-frequency time scales. Our secondary goal was to determine whether the southern Indian Ocean modes of variability are connected to Antarctic Oscillation. Notably, the AAO is the dominant pattern of nonseasonal tropospheric circulation variation south of 20°S, and it is characterized by pressure anomalies of one sign centered in the Antarctic and anomalies of the opposite sign centered around 40°–50°S. The recent trend in the Southern Hemisphere circulation is consistent with a systematic bias toward the high-index polarity of the AAO (Thompson and Solomon, 2002). In this study, it was also aimed to offer comprehensive insights into the southern Indian Ocean atmosphere–ocean coupled variability and to help the modeling studies associated with these programs.

The paper is organized as follows. A brief description of the datasets and methods is given in section 2. Section 3 introduces the main southern Indian Oceanic and atmospheric features. Section 4 presents the principal modes of behavior of the SST and the overlying atmospheric circulation in the southern Indian Ocean obtained from EOF analyses. The results pertaining to the atmosphere–ocean coupling based on the singular value decomposition (SVD) analysis are discussed in section 5, focusing on subtropical and mid-latitude regions. Finally, section 6 contains a summary and a discussion of the main results obtained from this study.

2. Data and methodology

2.1 *Data*

We used SST data from the Hadley Center. Sea level pressure, 850 hPa vector wind date were obtained from the European Centre for Medium-Range Weather Forecasts (ECMWF); heat fluxes were de-

rived from the National Centers for Environmental Prediction/National Center for Atmospheric Research (NCEP/NCAR) reanalysis dataset. These datasets are available as monthly means over the period January 1958 to June 2010. The geographical area of interest in our study is the southern Indian Ocean (55°S–equator, 30°–120°E). The climatology of these datasets were calculated for each calendar month at each grid point by averaging the data over 1958–2010. Monthly anomalies were then defined as deviations from this mean annual cycle.

The AAO index used in this study was downloaded from the National Weather Service Climate Prediction Center (http://www.cpc.ncep.noaa.gov/). The loading pattern of the AAO was defined as the first leading mode from the EOF analysis of monthly mean height anomalies in the South Hemisphere at 700 hPa (Mo, 2000). Year-round monthly mean anomaly data have been used previously to obtain the loading patterns. AAO indices were constructed by projecting the monthly mean 700-hPa height anomalies onto the leading EOF mode. In addition, the time series were normalized using the standard deviation of the monthly index (1979–2000).

2.2 *Methods*

EOF and SVD analyses were used to describe both the independent and coupled variability of SST and SLP in the Southern Indian Ocean. While the EOF analysis method has been widely applied in geophysics research (e.g., Wallace and Jiang, 1990; Deser and Blackmon, 1993), the SVD analysis method has become more commonly used only in the last decade. It is one of the most efficient ways to isolate the covariability between two fields (Wallace et al., 1992; Cheng and Dunkerton, 1995; Leuliette and Wahr, 1999). A brief description of the method follows here. Unlike EOF analysis, in which two variables are used separately, SVD is applied to the cross covariance matrix of them. Thus, the results describing the primary coherent mode cannot be assumed to represent the primary oscillation mode of variability for each individual field. The dominant modes explaining large fractions of squared covariance, with strong temporal and spatial correlations, are often interpreted in terms of dominant coherent modes of the data vectors. The heterogeneous correlation maps of the left and right fields, which are the correlation coefficient between the time series of the left modes with the right field and vice versa, not only provide a measure of coherent between the fields but also represent the causality between them in certain ways. For normalized input data, these heterogeneous correlation maps have the same patterns as the corresponding left and right singular vectors (Bretherton et al., 1992). Examples of the application of the SVD analysis are given in Bretherton et al. (1992) and Wallace et al. (1992). When the SVD analysis is performed, especially when the temporal dimension is far larger than the spatial, the resulted SVD modes are not always statistically significant, hence they do not have a physical explanation. Therefore, Shen and Lau (1995), Iwasaka and Wallace (1995) introduced the Monte Carlo technique to test the statistical significance of the SVD modes; Shi (1996) sketched the method that is also utilized in the present paper.

Notably, due to its limitations, the SVD, under certain circumstances, might produce paired patterns of no physical meaning (Newman and Sardeshmukh, 1995; Cherry, 1997; Hu, 1997). Cherry (1997) proposed that, prior to the use of SVD, an EOF analysis should be applied to each field to test whether the two sets of expansion coefficients from EOF analysis are strongly correlated and whether the patterns are geophysically relevant. Therefore, we conducted EOF analyses (see section 4) and tested whether such conditions were met.

In this method, the lead–lag correlation is employed to illustrate the potential causal relationship between two variables. Composite analysis is a common way to present the responses associated with a certain climate condition by averaging the data over the considered years. The Student's t-test is used to assess the statistical significance of the results obtained from composite and correlation analyses. The Morlet wavelet analysis (Torrence and Compo, 1998) and linear regression analyses were also utilized in this study.

3. Southern Indian Ocean atmosphere–ocean mean state

The mean summer and winter fields of SLP, 850-hPa vector wind, and SST, shown in Fig. 1, were used to compute the 52-year (1958–2010) climatology from the monthly means. Their distributions are displayed in Figs. 1a–c for austral wintertime (June–July–August, JJA) and in Figs. 1d–f and for summertime (December–January–February, DJF). The SLP and wind fields were dominated by the southern Indian Ocean subtropical high, whose centers were located near (30°S, 60°E) and (35°S, 90°E) in austral winter (Figs. 1a and b) and summer (Figs. 1d and e), respectively. The mean surface winds over the southern Indian Ocean were dominated by an anticyclone; north and south of 30°S the mean surface winds were predominantly easterly/westerly in associated with the subtropical high. These winds are more southeasterly off Australia during austral summer, when the

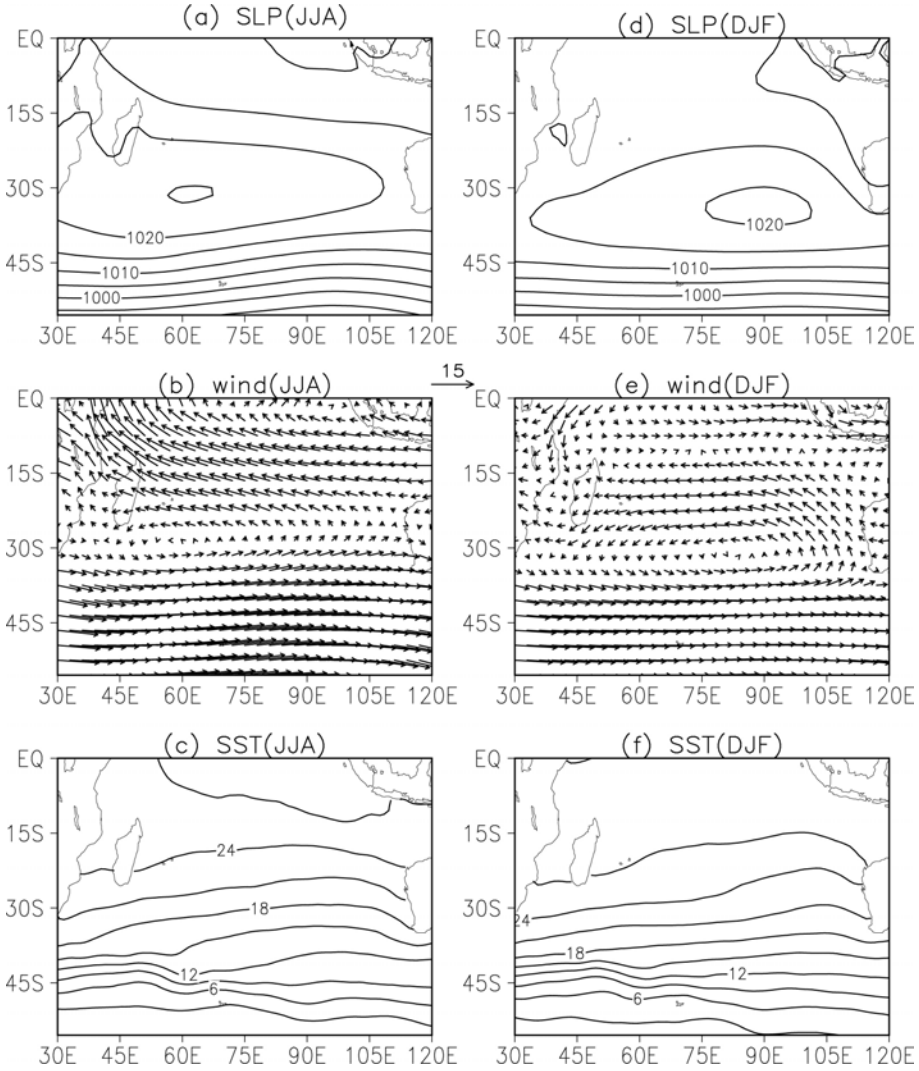

Fig. 1. Climatology fields for 1958–2010 austral winter of (a) SLP (in Pa), (b) 850-hPa wind (in m s^{-1}), and (c) SST (in °C) with contour interval 3°C. (d–f) The same as (a–c), but for austral summer (DJF).

center of the subtropical high shifts eastward. This circulation pattern is supported by the SLP distribution and gradients. The SST field exhibits a generally weak southwest–northeast gradient north of 35°S during both austral winter and summer (Figs. 1c and f). The isotherms extend zonally and are static all year south of this latitude. It is warmer during summer than winter because of solar radiation and Ekman drift induced by the surface wind.

4. The variability of SST and SLP: EOF analysis

In this section we present our EOF analyses of the SST and SLP fields of the variability of the oceanic surface temperatures and of the atmospheric sea level pressure during the 52-year period (1958–2010), conducted analyses. The product of pattern and time series gives the actual anomaly described by EOF or SVD. The pattern and time series are often called dominant modes and principal components (PC), respectively. Only these products have a physical meaning. By considering these dominant modes, we were able to compare the sets of EOF modes with the sets of SVD modes obtained for the coupled atmosphere–ocean system (see section 5). Only a brief discussion of the EOF mode is presented here because this study focused on the coupled modes.

4.1 *EOF analysis of SST*

The three leading EOF modes account for 51% of the total monthly SST variance. Individually, they ex-

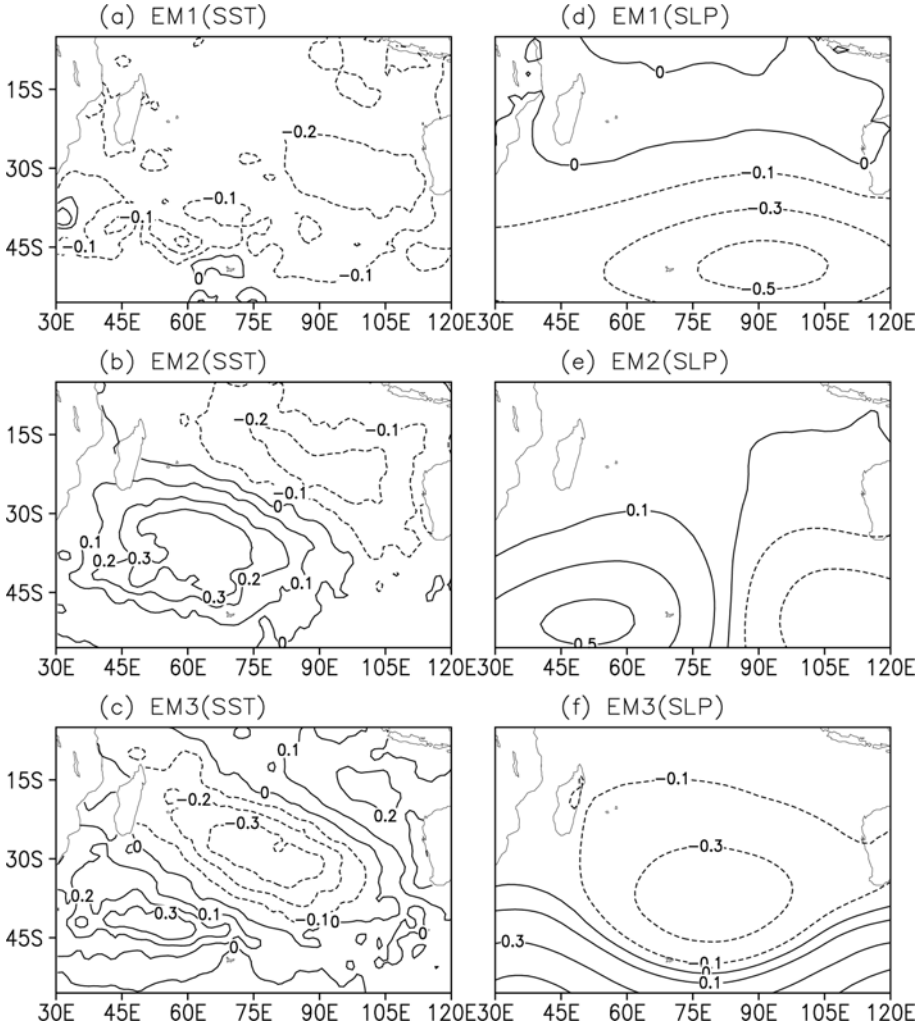

Fig. 2. Spatial patterns of (a) the first, (b) the second, (c) the third EOF modes of SST and (d–f) of SLP.

plain 28%, 13%, and 10% of the variance. The spatial patterns associated with the first three modes are depicted in Figs. 2a–c. They are labeled EM1 (SST), EM2 (SST), and EM3 (SST), respectively. Figures 3a–c shows the corresponding temporal variability of each EOF, represented by EPC1 (SST), EPC2 (SST), and EPC3 (SST), respectively.

EM1 (SST) (Fig. 2a) exhibits a monopole pattern extending over the entire domain. The largest loading was located in the mid-eastern region of the southern Indian Ocean, west of Australia. The result of our spectral analysis of EPC1 (SST) suggests that the first EOF mode oscillates on mainly a 25-year interdecadal time scale. The EPC1 (SST) also shows a secular trend, indicating the basin warming in past decades.

EM2 (SST) displays an out-of-phase relationship between temperature anomalies north and south of ∼25°S in a southwest–northeast direction (Fig. 2b). The northeast and southwest centers are located at 25°–15°S, 75°–105°E and 45°–30°S, 45°–75°E, respectively. Climatologically, isotherms are known to be nearly zonal in the southern Indian Ocean (Figs. 1c and f); the second EOF mode describes their north/south shift in a large area of the southwestern and northeastern region. The EPC2 (SST) is characterized by a mixture of interannual (∼3-year and ∼7-year periods) and interdecadal (∼25-year period) fluctuations. The SST pattern displayed here is broadly consistent with that found by Behera and Yamagata (2001) in their EOF analyses of the southern Indian Ocean. They referred to it as the Indian Ocean Subtropical Dipole (IOSD) and highlighted its independence from ENSO. Consistent with their results, a very weak correlation also exists between this mode and ENSO in this paper.

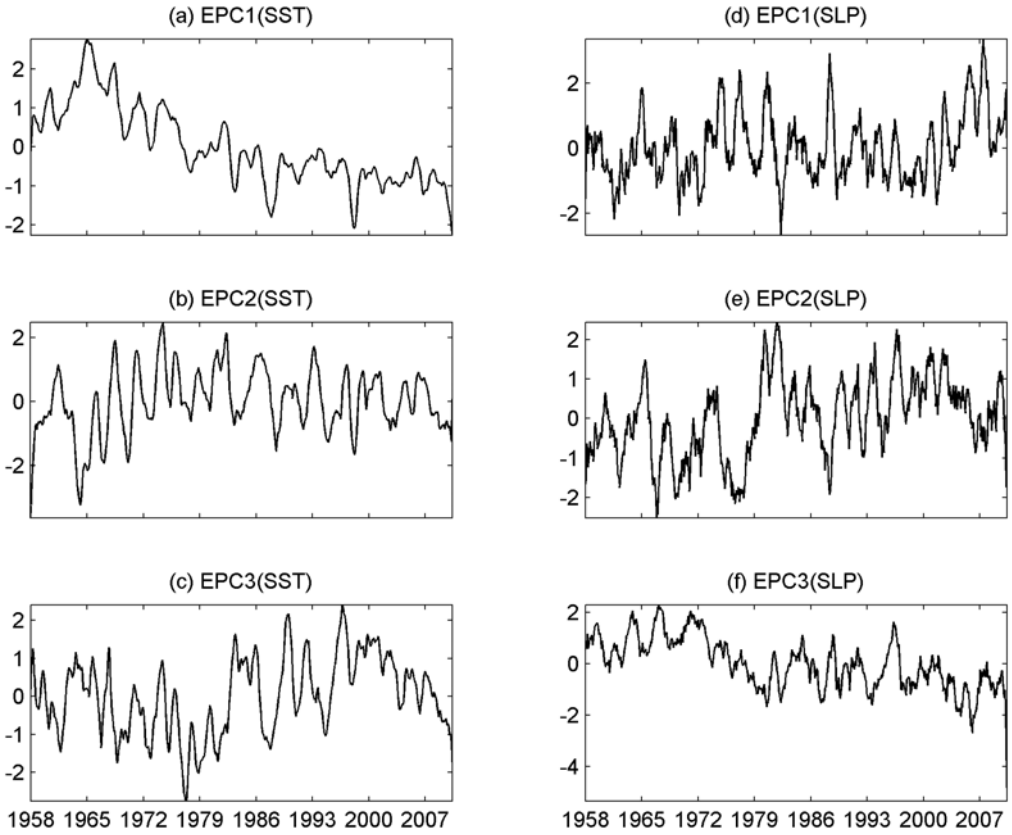

Fig. 3. Expansion coefficients of (a) the first, (b) the second, and (c) the third EOF modes of SST. (d–f) The same as (a–c), but for SLP field. Time series were smoothed by a 12-month running mean. Amplitudes were normalized by the standard deviation.

EM3 (SST) (Fig. 2c) exhibits three bands of centers of action with alternating signs in a southwest–northeast direction. The three loadings are centered at 45°–40°S, 45°–60°E; 40°–25°S, 70°–90°E; and 20°–15°S, 100°–110°E. Shown by the results of spectral analysis, the EPC3 (SST) is also characterized by a mixture of 8-year interannual and 16-year interdecadal fluctuations.

4.2 *EOF analysis of SLP*

A similar EOF analysis was performed for the monthly SLP anomalies over the same domain and time span as for SST anomalies. The first three EOF modes accounted for 75% of the total monthly SLP variance, with individual modes explaining fractions of 42%, 22%, and 11%. Figures 2d–f shows the spatial patterns of the first three modes, labeled EM1 (SLP), EM2 (SLP), and EM3 (SLP), respectively. Figures 3d–f shows their associated expansion coefficients, represented by EPC1 (SLP), EPC2 (SLP), and EPC3 (SLP), respectively.

The most variance, 42%, is explained by EM1 (SLP) (Fig. 2d). It is characterized by a single center located around 47°S, 90°E, south of 45°S. It describes a weakening and north–south displacement of the climatologically subtropical high, which was revealed by comparing this mode with climatologic field (Figs. 1a and d).

EM2 (SLP) (Fig. 2e) has a dipole structure in the east–west direction. It describes an east–west displacement of the subtropical high, and it suggests an anticorrelation between SLP in the eastern and western parts of the basin. Sterl and Hazeleger (2003) also found a similar SLP mode when they investigated SLP variability in the south Atlantic. Nevertheless, they argued that such a pattern was likely to be an artifact of the EOF technique. However, by composite analysis (figures not shown), we identified this robust seesaw signal in the southern Indian Ocean.

Similar to the first EOF mode, a giant low-pressure center also appeared in EM3 (SLP) (Fig. 2f) but with the center located the north of 45°S, which also demonstrates the strengthening and weakening of the subtropical high.

The spectrum of EPC1 (SLP) exhibits highly significant peaks at low-frequency oscillations of ∼25-year

Table 1. Correlation coefficients between the three first EOF modes of SST and SLP and between these modes and the AAO. Highly significant correlations exceeding the 99% confidence level are in bold and italicized face.

	EPC1 (SLP)	EPC2 (SLP)	EPC3 (SLP)	AAO
EPC1 (SST)	−0.04	0.00	***0.24***	−0.00
EPC2 (SST)	***−0.19***	0.09	***−0.25***	***0.21***
EPC3 (SST)	−0.04	***0.26***	0.001	−0.00
AAO	***−0.57***	0.03	−0.14	

period and interannual fluctuation of 3–4 years. The spectra of EPC2 (SLP) show predominantly an 8-year interannual fluctuation and a 16-year interdecadal oscillation. The spectra of EPC3 (SLP) show a significant peak at an interdecadal oscillation with a ∼25-year period.

4.3 *Relationship between ocean and atmosphere behaviors*

To look for possible links between oceanic and atmospheric fluctuations, the correlation coefficients between the PCs of the three leading SST and SLP modes were calculated (Table 1). As mentioned previously, the AAO is an important phenomenon of the Southern Hemisphere, and correlations with the time series of the AAO index were also included to test for possible links with the Antarctic Oscillation.

The simultaneous correlation between EPC2 (SST) and EPC1 (SLP) is −0.19, significant at the 99% confidence level. Therefore, the first mode of the atmospheric variability is related to the second mode of the ocean variability. Lagged correlations between these two expansion coefficients indicated that the two modes were correlated when the atmosphere led the ocean by 1–5 months (figures not shown), implying that the EM2 (SST) and EM1 (SLP) are linked via atmosphere-to-ocean forcing. To further confirm this hypothesis, we performed the following composite analysis of SST and SLP anomalies. From 1958 to 2010, positive EPC2 (SST) and negative EPC1 (SLP) >1 standard deviation (SD) co-occurred during the austral summers in the following years: 1961, 1972, 1982, 1994, 1997, 2006, and 2007 (Figs. 3b and d). Negative EPC2 (SST) and positive EPC1 (SLP) <1 SD co-occurred during the austral summers in the following years: 1958, 1964, 1992, and 1996. The composite maps of SST and SLP anomalies were created using the difference between the opposite phase events of these two groups. For simplicity, we selected the January case to represent the composite result (Fig. 4). We can see that Fig. 4a resembles the IOSD pattern of EM2 (SST). Figure 4b is similar to EM1 (SLP), which also describes changes of subtropical high. Therefore, the second EOF mode of SST is indeed related to the first EOF mode of SLP. In the next section, further evidence supports the conclusion that these results derive from atmosphere–ocean coupled processes.

Both the EPC1 (SST) and EPC2 (SST) are significantly correlated with EPC3 (SLP), the coefficients are 0.24 and −0.25, respectively. The EPC3 (SST) and EPC2 (SLP) are related with each other quite faithfully, with a correlation of 0.26 at a 99% confidence level.

Because the first SLP pattern is somewhat similar to the AAO mode, we anticipated possible links between them. To determine these links, we performed the lead–lag correlation analysis between EPC1 (SLP) and the AAO index. Our results show that significant correlations, with values exceeding 0.4, appear

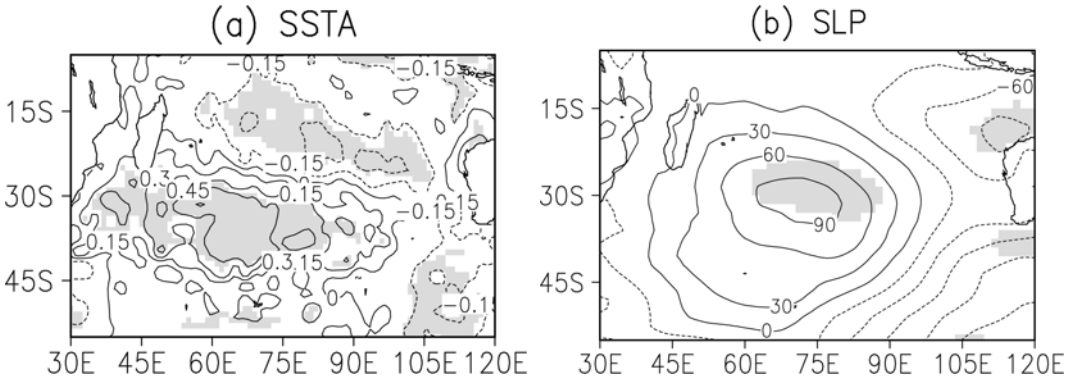

Fig. 4. Composites of (a) SST and (b) SLP anomalies during the peak phase for difference between seven positive peak in EPC2 (SST) when EPC1(SLP) is in negative peak and four negative peak in EPC2(SST) when EPC1(SLP) is in positive peak during 1958–2010. Counter interval is 0.15°C for the SST anomaly and 30 hPa for the SLP anomaly. Shading denotes values exceeding the 95% confidence level.

when AAO leads SLP by −2 to 1 months. The most significant correlation coefficient of −0.57 appears at zero lag, indicating that this mode is highly associated with the AAO. In addition, the EPC2 (SST) was also found to be significantly correlated with the AAO.

The relationship revealed by these significant correlations is further explored in the next section.

5. SVD analysis of SST and SLP

To assess and confirm the relationships between SST and SLP variations, SVD analysis was performed on the cross-covariance matrix between them. To examine the statistical robustness of the results obtained from the SVD analysis, we performed a significance test using a Monte Carlo approach. Our results show that the first two modes for each pair of variables are well beyond the 95% confidence level. The covariance is also strongly concentrated in the first two modes, which isolate large-scale spatial features with low-frequency time scales. They independently explain 43% and 30% of the total square covariance, respectively. The coupled spatial patterns and expansion coefficients corresponding to each variable of the first two modes are displayed in Figs. 5 and 6. The SST/SLP spatial patterns are labeled as SM1 (SST)/SM1 (SLP) and SM2 (SST)/SM2 (SLP), respectively. The corresponding time series of expansion coefficients are SPC1 (SST)/SPC1 (SLP) and SPC2 (SST)/SPC2 (SLP), respectively. They are discussed separately in the following sections.

5.1 *The first SVD mode*

Figures 5a and c shows the components of the first SVD modes of the coupled fields. Figure 6a displays the corresponding expansion coefficients. The SST mode displays an out-of-phase relationship between temperature anomalies north and south of ∼30°S, in a southwest–northeast direction. The centers are located at 30°–20°S, 75°–100°E and 45°–35°S, 45°–75°E, respectively. The SLP mode (Fig. 5c) has a monopole structure, which is related to changes of subtropical high. It describes the north–south displacement of the climatologically subtropical high.

The spectral analysis on both SPC1 (SST) and SPC1 (SLP) shows that the time series is characterized by a mixture of 3-year inter-annual and 25-year interdecadal fluctuations (Fig. 7a).

The SST pattern and time series closely resemble those of EM2 (SST), but with a slightly southward dis-

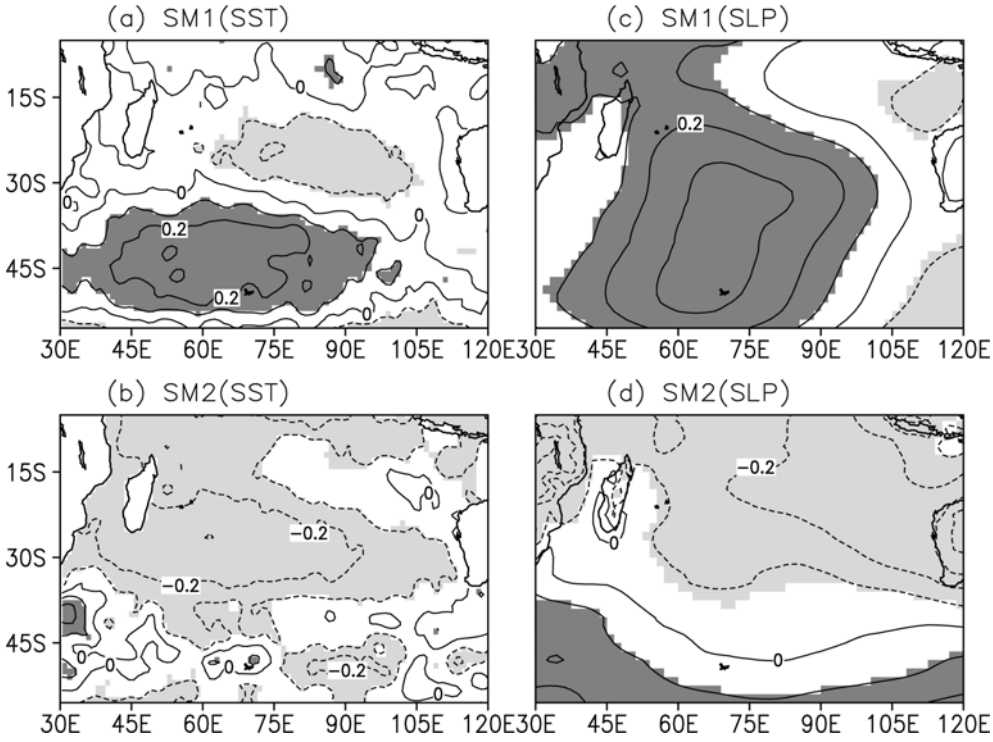

Fig. 5. Heterogeneous correlation patterns of the first two leading SVD mode for the (a–b) SST and (c–d) SLP. Values with positive correlation coefficients that are significant at the 99% confidence level are shaded dark; values with a negative correlation are indicated by light shading.

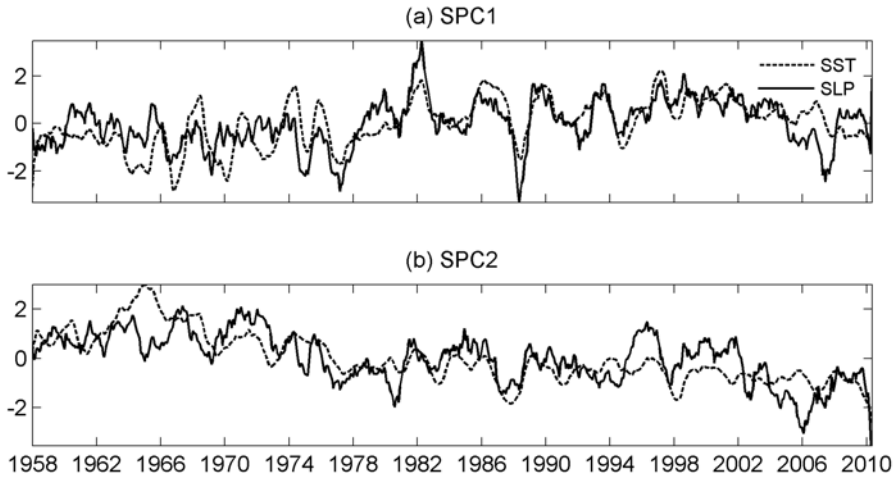

Fig. 6. Expansion coefficients of (a) the first and (b) the second SVD modes of SST (dashed line) and SLP (solid line). Time series were smoothed by a 12-month running mean. Amplitudes were normalized by the standard deviation.

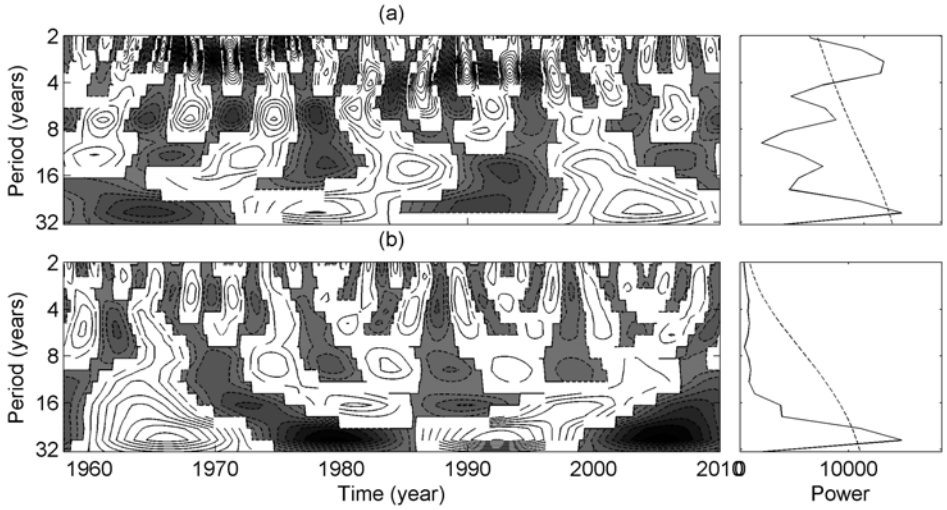

Fig. 7. Wavelet analyses of (a) the first and (b) the second time series of SVD mode of SST and SLP. The left panel shows the real part of wavelet analysis. Negative values are shaded. The left axis is the Fourier period (in years). And the right panel refers to the global wavelet spectrum of the time series, with dashed line denoting the 99% confidence level.

placement of the northern activity center. Moreover, correlation between EPC2 (SST) and SPC1 (SST) is as high as 0.97, indicating that the SM1 (SST) is identical to IOSD mode. Therefore, the SST associated with the first SVD mode is the important coherent large scale pattern in the southern Indian Ocean in its own right. We still denote SM1 (SST) as IOSD in the following text. Positive IOSD is defined by negative and positive SST anomalies in the north and south 30°S, respectively. In contrast to the SST mode, the SLP pattern does not appear as clearly from the independent EOF analyses. However, it still represents north–south displacement of the climatologically subtropical high. And the SM1 (SLP) pattern resembles the composite maps of SLP anomalies based on EPC1 (SLP) shown in Fig. 4b. Furthermore, the correlation between EPC1 (SLP) and SPC1 (SLP) is as high as −0.74, far exceeding 99.9% confidence level. In addition, the spectra of the SPC1 (SLP) is almost identical to that of EPC1 (SLP). Hence, the first atmosphere–ocean coupled mode is related to the correlation found between EPC2 (SST) and EPC1 (SLP), −0.19, which is not very high but is significant at 99% confidence level.

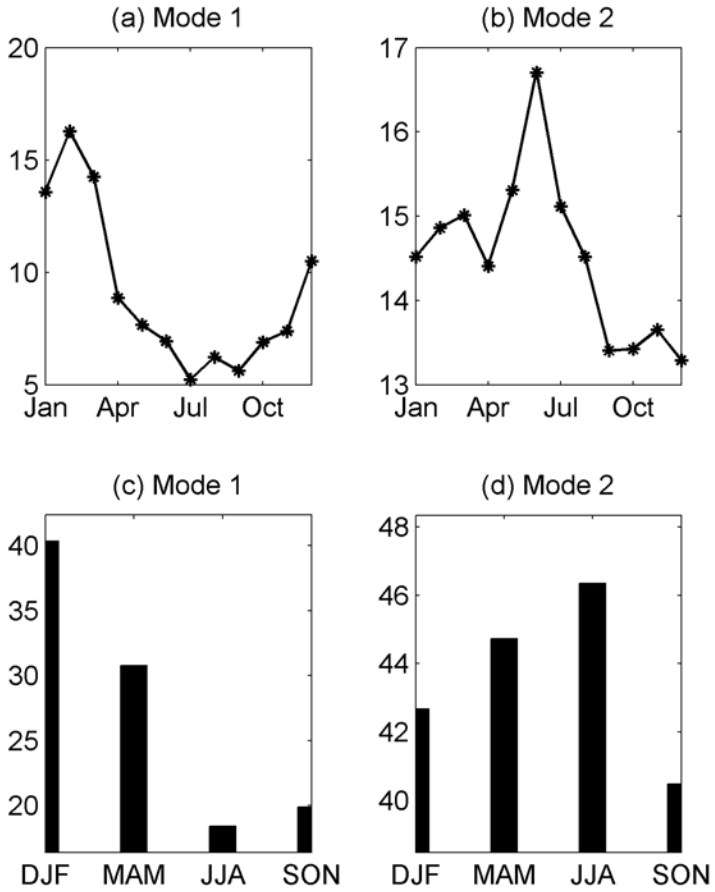

Fig. 8. Standard deviation of monthly time series of (a) the first and (b) the second SVD modes of SST. (c) and (d) show the seasonal totals of (a) and (b), respectively.

To examine the seasonality of this mode, we calculated the standard deviation of the time series of expansion coefficients for each calendar month and each season. Results are shown in Fig. 8. Figures 8a and c indicates that the coupled variability is the strongest during the austral summer (DJF), which was also noted by Behera and Yamagata (2001). It is likely that the seasonality in the data coverage may account in part for the strong coupling in different seasons. To illustrate this result, we also performed the SVD analysis on the year-by-year summer (average of DJF) SST and SLP. The first SVD mode is the same as presented here (figures not shown). Similar SST and SLP spatial patterns are also reported in Huang and Shukla (2008), who conducted canonical correlation analysis (CCA) between the DJF mean SST and SLP anomalies for 1950–2000 in this region. Thus, the first SVD SST mode is indeed closely related to the second EOF SST mode.

To better assess and confirm the relationships between ocean and atmosphere, the lead–lag correlation coefficients between the expansion time series of the two variables are displayed in Fig. 9. The lead–lag correlations can be applied to examine the potential causal relationships between SST and SLP anomalies. Significant correlations (values >0.4), appear when SLP leads SST by 4 to -1 months (Fig. 9a). The strongest interaction between them appeared when SLP led SST by 1–2 months, implying an atmosphere-to-ocean forcing. This result is consistent with that from EPC1 (SLP) and EPC2 (SST).

By comparing the patterns of SM1 (SST), SM1 (SLP) (Figs. 5a and c), and climate fields (Figs. 1a and d), we can see that warm anomalies in the southwest are mainly accompanied by a southwestward shift and a strengthening of the Mascarene high. To further examine the potential physical processes, we applied the linear regression analyses between the 850-hPa wind field, heat fluxes, and the SPC1 (SLP). Regressed maps of wind and heat fluxes are shown in

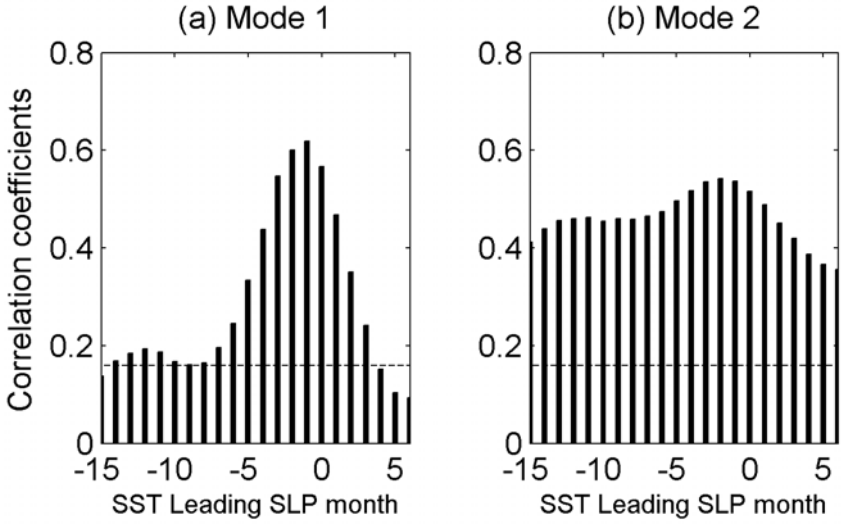

Fig. 9. Lead–lag correlations between the two time series of (a) the first and (b) the second SVD modes. SLP leads SST for negative lags, and SLP lags SST for positive lags. Dashed line shows the 99% confidence level.

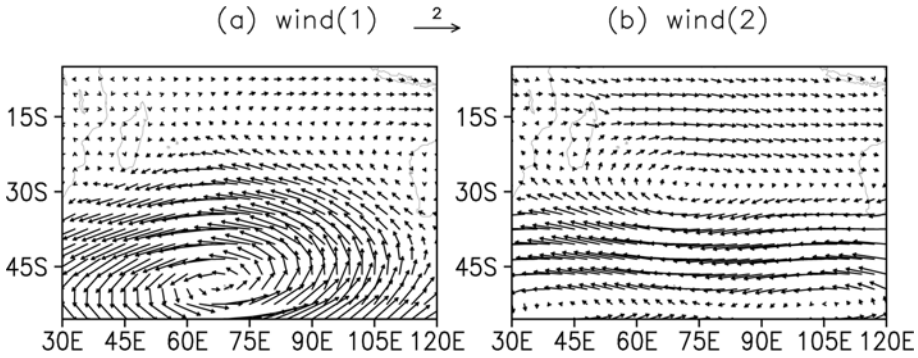

Fig. 10. Linear regression fields of 850-hPa wind vector against the PCs of (a) the first and (b) the second SVD SLP modes (in m s^{-1}).

Figs. 10 and 11, respectively. A comparison of the SM1 (SLP) (Fig. 5c) and the regressed 850-hPa wind (Fig. 10a) shows that a high-pressure center south of 30°S corresponds to an easterly wind anomaly band along 45°–30°S, indicating a weakening of the climatologically westerly wind (Figs. 1b and e). Suzuki et al. (2004) also proved this observational fact in a coupled general circulation model.

Interestingly, the pattern of net heat flux (Fig. 11a), to which the latent heat flux (Fig. 11b) contributes much, resembles the structure of SM1 (SST) (Fig. 5a). This implies that the heat flux must be a main contributor of the SST variation. A strong relation between the surface heat flux and the atmospheric variables is expected; surface heat flux is determined by surface wind speed, atmosphere–ocean temperature difference, and specific humidity difference. Due to the position and strength modifications of the subtropical high, the wind field changed. On one hand, the weaker-than-normal wind results in smaller-than-normal ocean-to-atmosphere latent and sensible heat fluxes (Figs. 11b and c), which produces a zonally oriented, positive SST anomaly south of 30°S. On the other hand, over the northern activity center, particularly along the 30°–15°S band east of 70°E, the stronger-than-normal southeast wind resulted in more latent and sensible heat fluxes from ocean to atmosphere (Figs. 11b, c), thus forming a negative SST anomaly. Chiodi and Harrison (2007) proposed that this latent heat flux variability is mainly caused by near-surface humidity variability, which is fundamentally driven by the anomalous meridional advection of water vapor. Suzuki et al. (2004) showed that the latent heat flux anomalies influence SST anomalies more

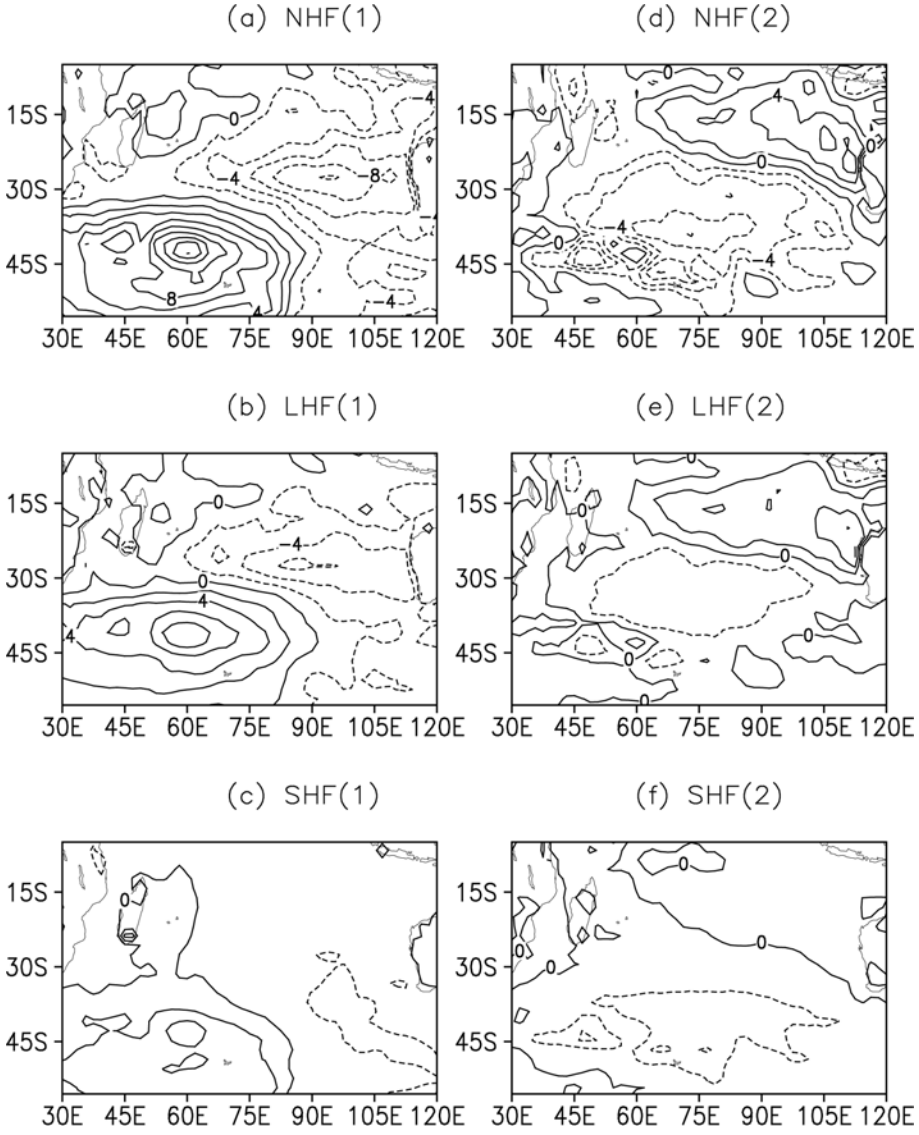

Fig. 11. Linear regression fields of (a) the net heat flux (NHF), (b) latent heat flux (LHF), and (c) sensible heat flux (SHF) against the first SVD SLP time series. (d–f) are the same as (a–c), except for the second modes, respectively. The contour interval is 2. Positive values mean that the ocean gains heat, and negative values mean that the ocean loses heat.

efficiently when the surface mixed-layer becomes shallow. In addition to the latent heat flux, our results in the present study show that the contribution of the sensible heat flux to the SST variation is not negligible. However, Morioka et al. (2010) suggest that contribution from shortwave radiation is most dominant in the growth of IOSD SST anomalies, in which the mixed-layer thickness anomaly has an important role, whereas the contribution of the latent heat flux to the SST variation is not important. Thus, there is still disagreement regarding this issue.

As we know, the current in the upper ocean is dominated by the Ekman flow induced by the surface wind stress (Carton et al., 2000a, b); the oceanic processes induced by the wind field (Fig. 10a) must have a significant influence on the SST variation. The strong easterly wind in the southwest of the southern Indian Ocean makes the relatively warmer water north of 30°S accumulate to the south of 30°S region through the meridonal advection, which is associated with Ekman flow. In addition, the downwelling induced by the anti-cyclonic circulation south of 30°S also contributes to the positive SSTA. North of 30°S, the Ekman upwelling associated with the cyclonic circulation in the

eastern region, to the west coast of Australia, also has some contribution to the negative SSTA.

In summary, these characteristics of the wind–SST relationship reveal that wind-induced mechanisms, including heat flux variation and Ekman upwelling or downwelling processes, drive the variations in the ocean temperature. In return, the dipole pattern of the ocean temperature enhances the behavior of the overlying atmospheric, though not very strongly; the significant correlation between the two time series of expansion coefficients (Fig. 9a) only appeared when SST led SLP by 1–3 months. By employing a general circulation model, Reason and Godfred-Spenning (1998) also found that the response of the atmosphere to an idealized SST anomaly (warm in southern midlatitudes, cool in southern tropics), similar to the IOSD pattern, can lead to changes in surface heat fluxes and in the strength of the south Indian subtropical gyre that opposes the original SST anomaly. Our results are in good agreement with the model results suggested by Reason and Godfred-Spenning (1998).

5.2 *The second mode*

Figures 5b and d shows the second SST and SLP modes, respectively. The corresponding expansion coefficients are depicted in Fig. 6b. The SST mode exhibits a monopole pattern extending over the entire domain and is similar to the first EOF mode pattern of SST, but it has a large amplitude in a band extending westward from the west coast of Australia to the region east of Madagascar along 30°S. The SLP also has uniform polarity over the entire domain. The activity center of the mode is located near the center of the subtropical high (Figs. 1a, d). This mode also describes the strengthening and weakening of the anticyclone.

The results of our spectral analysis on both the SST and SLP expansion coefficients of the second SVD mode (Fig. 6b) indicate a dominant spectral peak at ∼25 years (Fig. 7b). Negative values were seen in the 1960s and 1990s, while positive ones were seen in the late 1970s to early 1980s and 2000s. A negative trend was also detected in both SST and SLP time series during 1958–2010, implying the secular basin-warming of SST and long-term SLP increasing in variation, particularly along the north edge of subtropical high. This variation may arise through a combination of basin scale atmosphere–ocean interaction and a remotely forced component (Reason et al., 1998).

The SST time series also compared well with EM1 (SST) (Fig. 2a). The SLP time series and pattern for the second SVD mode compared well with the third EOF mode of SLP (Fig. 2f). The correlation coefficient was 0.56 between EPC3 (SLP) and SPC2 (SLP) and was 0.75 between EPC1 (SST) and SPC2 (SST). So this mode is related to the correlation found between EPC1 (SST) and EPC3 (SLP) (Table 1).

From Figs. 8b and d, we can see that this mode also shows strong seasonal variation and is active during the austral winter (JJA). This is further confirmed by applying SVD analyses of year-by-year SST and SLP during winter (average of JJA). The first mode also presents the same characters in both spatial pattern and frequency features.

To investigate possible air–sea forcing mechanisms related to the second SVD mode, we examined the lead–lag correlation between the two time series, the linear regression field of wind, and the heat fluxes associated with it. The high degrees of correlation (Fig. 9b) between SPC2 (SST) and SPC2 (SLP) indicate strong oceanic response to atmosphere nearly simultaneously, while the value is slightly higher when the SLP leads the SST by 1–2 months. Previous researchers (Deser and Blackmon, 1993; Kushnir, 1994) concluded from investigations of the North Atlantic that interannual variability is primarily driven by the atmosphere, while interdecadal or longer-scale variability is mainly associated with changes in the ocean. However, recently some other studies of the Atlantic Ocean have suggested that atmospheric-to-ocean forcing on interdecadal time scales may be more important (e.g., Halliwell, 1996; Venegas et al., 1997). The lead–lag correlation presented here somewhat supports this idea. In a word, the subsidence of atmosphere is the main reason for the formation of the second SVD mode.

To understand the details of oceanic response to the atmosphere, we next compared the SST pattern with the wind regression map (Fig. 10b). A giant cyclone, with the center located along 28°S (Fig. 10b), corresponding to the low SLP in Fig. 5d, can be seen just over the strong cold SSTA center (Fig. 5b). Because of such cyclonic circulation, temperature and humidity differences between ocean and atmosphere become larger. Consequently, the latent and sensible heat fluxes increase, thus the ocean loses heat south of 28°S (Figs. 11d–f). In addition, Ekman upwelling caused by this strong cyclone also contributes to the SST cooling.

However, northwest of the Australia (Fig. 11d), the ocean gains heat from the atmosphere–ocean interface mainly because of the reduced latent and sensible heat flux from ocean to atmosphere (Figs. 11e, f), which is due to the weak-than-normal wind, whereas the SSTA remains negative there. Thus the heat flux is no longer a reason for the SST cooling. From Fig. 10b, we can see that the northern branch of cyclone circulation north of 28°S is dominated by westerly anomalies.

This westerly can induce a cold temperature advection from mid-latitude to the low latitude by Ekman drift current. Furthermore, the northern branch of the cyclone can also make the relative cold water in the western part of southern Indian Ocean accumulate to the eastern warm pool region by advection, contributing to the negative SSTA there. Consequently, the negative SSTA to the northwest of Australia is mainly due to the oceanic process forced by the overlying atmosphere.

5.3 *Connection between AAO and coupled variability*

As we know, the AAO is the dominant pattern of tropospheric circulation variation in the mid-high latitudes of the Southern Hemisphere. We anticipated a linkage between AAO and the covariability in the southern Indian Ocean. Lagged temporal correlations of the time series of expansion coefficients and AAO index corroborate this connection (Fig. 12). We found that the highest correlation (0.57, significant at 99.9% confidence level), between SPC1 (SLP) and AAO index, corresponds to the zero lag, suggesting that the first atmosphere–ocean coupled mode is associated with AAO. Because previous results have shown that both EPC2 (SST) and EPC1 (SLP) are highly correlated with AAO (Table 1), this result is not surprising.

To further examine the relationship between the first coupled mode and AAO, composites of the SLP anomalies corresponding to the 9 positive and 12 negative maximum values of SPC1 (SLP) were studied

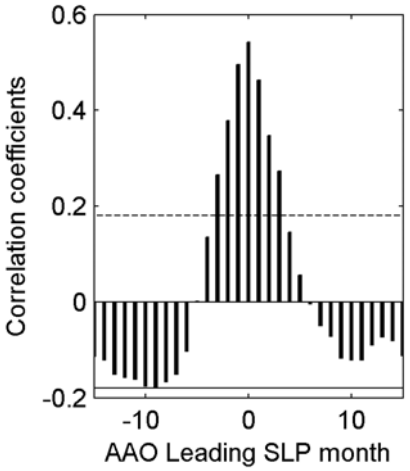

Fig. 12. Lead–lag correlations between AAO index and SLP time series of the first SVD mode. SLP leads AAO for negative lags, and SLP lags AAO for positive lags. Dashed line shows the 99% confidence level.

(Figs. 13a and b). These two composites describe the atmosphere conditions in the positive and negative peak conditions, which are exactly the positive and negative phases of AAO. The corresponding SST anomaly composites are positive and negative IOSD patterns (figures not shown). Again, these results show that the primary coupled mode of the southern Indian Ocean depicts an oscillation between strengthening and weakening of the subtropical high because of the variation of westerly along 45°–30°S, which is associated with AAO. The coincidence between them indicates that the atmosphere component of the coupled mode may be a part of AAO. This result therefore emphasizes the potential strong control of AAO on the variability of atmosphere–ocean coupled process in the southern Indian Ocean. In fact, Hermes and Reason (2005) demonstrated that the relationship between AAO and subtropical dipole mode in the southern Indian Ocean is apparent, which is in agreement with our results. However, some differences remain. Hermes and Reason showed that the wavenumber-3 or -4 pattern in the mid-latitude was visible, which is not illustrated in our study (Fig. 13). Moreover, the atmosphere–ocean covariability associated with IOSD has also been shown to connect with AAO in this study.

How does the dominant covariability in the southern Indian Ocean relate to AAO? As we know, the AAO pattern is related to the zonal mean zonal wind indices. It is associated with the zonal wind pattern with a maximum near 60°S and a minimum near 40°S (Kidson, 1988), which is vividly shown in Fig. 13. The SLP pattern shown in Fig. 13a implies the weakening of the westerly jet over the south edge of Mascarene high and strengthening of the easterly jet at high latitudes. This is consistent with the 850-hPa wind anomalies regressed upon SPC1 (SLP) (Fig. 10a). There are more zonal mean westerly anomalies over high latitudes (45°–60°S) and less westerly anomalies over the subtropics (30°–45°S). Hence, the Mascarene high strengthens. IOSD mode emerges in the southern Indian Ocean through atmosphere–ocean coupled processes.

6. Discussion and conclusions

In this paper, we have documented the results of our study of the interannual and interdecadal atmosphere–ocean covariability as well as the mechanisms behind it in the southern Indian Ocean. Using statistical methods, we have identified and described the main patterns of coupled and uncoupled surface variability by investigating how the system varies. These variables are linked with each other through ther-

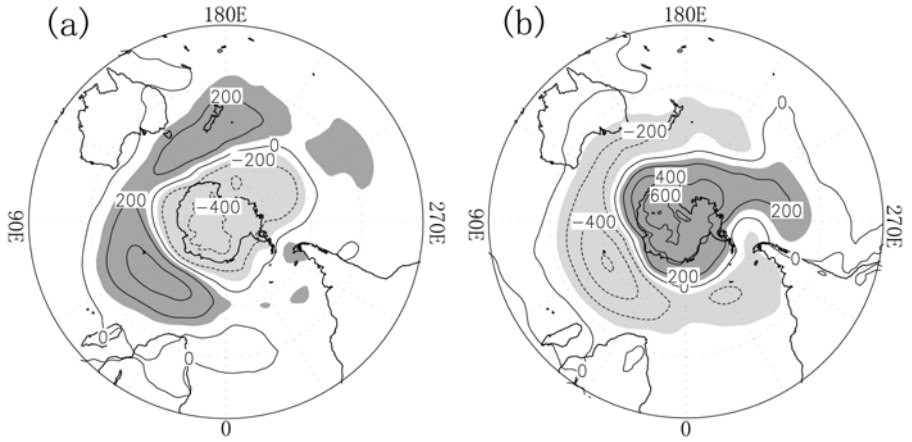

Fig. 13. SLP composite map corresponding to the highest (a) positive and (b) negative values of SPC1(SLP). The dark and light shaded areas are significant at the 99% confidence level for positive and negative values, respectively. The counter interval is 200 hPa.

modynamic like heat flux momentum, in which the latent and sensible heat fluxes are dominant. Variations of such variables depend not only on the heat flux momentum but also on oceanic processes such as Ekman flow and advection. The relationship between ocean and atmosphere discussed in this paper is mainly local and qualitative. The quantitative aspect calls for further exploration using numerical experiments.

The first two leading SVD modes of SST and SLP fields in the southern Indian Ocean, together accounting for 73% of the total variance, have been identified. The primary mode is characterized by weakness of the subtropical anticyclone, which seems to force fluctuations in a subtropical dipole structure in the SST: the southwestern part at the mid-latitude and the northeastern part at subtropical latitudes. A possible relationship between this mode and AAO has been revealed. AAO can influence atmosphere–ocean condition in the southern Indian Ocean by modulating the Mascarene high. Huang and Shukla (2008) also found that the extra-tropical atmospheric anomaly associated with AAO forces surface heat flux anomalies and results in SST anomalies related to the subtropical dipole in austral spring, summer, and fall. In addition, our results show that the same case also appears in austral winter, although the strongest covariability occurs in austral summer. The model results of Huang and Shukla show the initial atmospheric fluctuations are associated closely with AAO, but their observed results demonstrate the fluctuations are significantly correlated to ENSO. However, our results are consistent with their model results. Behera and Yamagata (2001) also considered that the subtropical dipole does not connect with ENSO. The differences among different results call for further exploration.

The basin-scale oscillations in the second SVD mode occur on a 25-year inter-decadal time period. This mode is forced by the atmosphere and mainly results in the subsidence. The periodic decadal oscillation found in this study is on a 25-year time scale. As shown in Figs. 7a and b, two complete episodes with positive and negative phases occurred in the past 50 years. In a couple of years, another positive phase episode appears in the southern Indian Ocean, the leading SST anomaly patterns on the interdecadal time scale are characterized by a cold basin (2nd SVD mode) and a negative IOSD (1st SVD mode).

Importantly, we only considered the processes that are active in the interface of ocean and atmosphere to understand the coupled mechanism, and the explanations given here are qualitative; some physical processes are still unclear. In fact, as documented in several studies (e.g., Shannon et al., 1990; Allan et al., 1995; Mason, 1995; Reason et al., 1996), the ocean circulation in Southern Indian Ocean also displays significant variability in SST on intraseasonal through to multidecadal time scales. The oceanic process should receive more attention in the future for understanding the large-scale climate system.

Acknowledgements. This study was supported by the Major Project of the National Natural Science Foundation of China (Grant No. 40890151) and the National Natural Science Foundation of China (Grant No. 41106016).

REFERENCES

Allan, R. J., J. A. Lindesay, and C. J. C. Reason, 1995: Multidecadal variability in the climate system over the Indian Ocean region during the austral summer.

J. Climate, **8**, 1853–1873.

Behera, S. K., and T. Yamagata, 2001: Subtropical SST dipole events in the southern Indian Ocean. *Geophys. Res. Lett.,* **28**, 327–330.

Bretherton, C. S., C. Smith, and J. M. Wallace, 1992: An intercomparison of methods for finding coupled patterns in climate data. *J. Climate,* **5**, 541–560.

Carton, J. A., G. Cherupin, X. Cao, and B. Giese, 2000a: A simple ocean data assimilation analysis of the global upper ocean 1950–1995. Part I: Methodology. *Journal of Physical Oceanography,* **30**, 294–309.

Carton, J. A., G. Cherupin, X. Cao, and B. Giese, 2000b: A simple ocean data assimilation analysis of the global upper ocean 1950–1995. Part II: Results. *Journal of Physical Oceanography,* **30**, 311–326.

Cheng, X., and T. J. Dunkerton, 1995: Orthogonal rotation of spatial patterns derived from singular value decomposition analysis. *J. Climate,* **8**, 2631–2643.

Cherry, S., 1997: Some comments on singular value decomposition analysis. *J. Climate,* **10**, 1759–1761.

Chiodi, A. M., and D. E. Harrison, 2007: Mechanisms of summertime subtropical southern Indian Ocean Sea surface temperature variability: On the importance of humidity anomalies and the meridional advection of water vapor. *J. Climate,* **20**, 4835–4852.

Deser, C., and M. L. Blackmon, 1993: Surface climate variations over the North Atlantic Ocean during winter: 1900–1989. *J. Climate,* **6**, 1743–1753.

Fauchereau, N., S. Trzaska, Y. Richard, P. Roucou, and P. Camberlin, 2003: Sea-surface temperature co-variability in the southern Atlantic and Indian Oceans and its connections with the atmospheric circulation in the southern hemisphere. *Int. J. Climatol.,* **23**, 663–677.

Goddard, L., and N. E. Graham, 1999: Importance of the Indian Ocean for simulating rainfall anomalies over eastern and southern Africa. *J. Geophys. Res.,* **104**, 19099–19116.

Halliwell, G. R., 1996: Atmospheric circulation anomalies driving decadal/interdecadal SST anomalies in the North Atlantic. *ACCP Notes,* **III**(1), 8–11.

Hermes, J. C., and C. J. C. Reason, 2005: Ocean model diagnosis if interannual coevolving SST variability in the southern Indian and south Atlantic Oceans. *J. Climate,* **18**, 2864–2882.

Hu, Q., 1997: On the uniqueness of the singular value decomposition in meteorological applications. *J. Climate,* **10**, 1762–1766.

Huang, B. H., and J. Shukla, 2007: Mechanisms for the interannual variability in the tropical Indian Ocean. Part II: Regional processes. *J. Climate*, **20**, 2937–2960.

Huang, B. H., and J. Shukla, 2008: Interannual variability of the South Indian Ocean in observations and a coupled model. *Indian Journal of Marine Sciences*, **37**, 13–34.

Iwasaka, N., and J. M. Wallace, 1995: Large scale air sea interaction in the Northern Hemisphere from a view point of variations of surface heat flux by SVD analysis. *J. Meteor. Soc. Japan,* **73**, 781–794.

Kidson, J. W., 1988: Interannual variations in the Southern Hemisphere circulation. *J. Climate*, **1**, 1177–1198.

Kushnir, Y., 1994: Interdecadal variations in North Atlantic sea surface temperature and associated atmospheric conditions. *J. Climate,* **7**, 141–157.

Latif, M., and T. P. Barnett, 1996: Decadal climate variability over the North Pacific and North America: Dynamics and predictability. *J. Climate,* **9**, 2407–2423.

Leuliette, E. W., and J. M. Wahr, 1999: Coupled pattern analysis of sea surface temperature and TOPEX/Poseidon sea surface height. *J. Phys. Oceanogr.*, **29**, 599–611.

Liu, N., Z. Jia, H. X. Chen, F. Hua, and Y. F. Li, 2006: Southern high latitude climate anomalies associated with the Indian Ocean dipole mode. *Chinese Journal of Oceanology and Limnology,* **24**, 125–128.

Mann, M. E., and J. Park, 1996: Joint spatiotemporal modes of surface temperature and sea level pressure variability in the Northern Hemisphere during the last century. *J. Climate,* **9,** 2137–2162.

Mason, S. J., 1995: Sea-surface temperature—South African rainfall associations, 1910–1989. *Int. J. Climatol.,* **15**, 119–135.

Mo, K. C., 2000: Relationships between low-frequency variability in the Southern Hemisphere and sea surface temperature anomalies. *J. Climate,* **13**, 3599–3610.

Morioka, Y., T. Tozuka, and T. Yamagata, 2010: Climate variability in the southern Indian Ocean as revealed by self-organizing maps. *Climate Dyn.*, **35**, 1059–1072.

Nan, S. L., J. P. Li, X. J. Yuan, and P. Zhao, 2009: Boreal spring Southern Hemisphere annular mode, Indian Ocean sea surface temperature, and East Asian summer monsoon. *J. Geophys. Res.,* **14**, D02103, doi: 10.1029/2008JD01 0045.

Newman, M., and P. Sardeshmukh, 1995: A caveat concerning singular value decomposition. *J. Climate,* **8**, 352–360.

Reason, C. J. C., 1999: Interannual warm and cool events in the subtropical mid-latitude south Indian Ocean region. *Geophys. Res. Lett.,* **26**, 215–218.

Reason, C. J. C., 2001: Subtropical Indian Ocean SST dipole events and southern African rainfall. *Geophys. Res. Lett.,* **28**, 2225–2227.

Reason, C. J. C., 2002: Sensitivity of the southern African circulation to dipole sea-surface temperature patterns in the south Indian Ocean. *Int. J. Climatol.,* **22**, 377–393.

Reason, C. J. C., and C. R. Godfred-Spenning, 1998: SST variability in the South Indian Ocean and associated circulation and rainfall patterns over Southern Africa. *Meteorology and Atmospheric Physics,* **66**, 243–258.

Reason, C. J. C., and H. Mulenga, 1999: Relationships between South African rainfall and SST anomalies

in the southwest Indian Ocean. *Int. J. Climatol.,* **19**, 1651–1673.

Reason, C. J. C., R. J. Allan, and J. A. Lindesay, 1996: Evidence for the influence of remote forcing on interdecadal variability in the southern Indian Ocean. *J. Geophys. Res.,* **101**, 11876–11882.

Reason, C. J. C., C. R. Godfred-Spenning, R. J. Allan, and J. A. Lindesay, 1998: Air-sea interaction mechanisms and low frequency climate variability in the South Indian Ocean region. *Int. J. Climatol.,* **18**, 391–405.

Rocha, A., and I. Simmonds, 1997a: Interannual variability of south–eastern African summer rainfall. Part 1: Relationships with air-sea interaction processes. *Int. J. Climatol.,* **17**, 235–265.

Rocha, A., and I. Simmonds, 1997b: Interannual variability of south–eastern African summer rainfall. Part 2: Modelling the impact of seasurface temperatures in rainfall and circulation. *Int. J. Climatol.,* **17**, 267–290.

Shannon, L. V., J. J. Agenbag, N. D. Walker, and J. R. E. Lutjeharms, 1990: A major perturbation in the Agulhas retroflection area in 1986. *Deep-Sea Res.*, **3**, 493–512.

Shen, S., and K. M. Lau, 1995: Biennial oscillation associated with the East Asian summer monsoon and tropical sea surface temperatures. *J. Meteor. Soc. Japan,* **73**, 105–124.

Shi, N., 1996: Confidence test of SVD method in the study of climate diagnose. *Meteorological Science and Technology,* **4**, 5–6. (in Chinese)

Sterl, A., and W. Hazeleger, 2003: Coupled variability and air-sea interaction in the South Atlantic Ocean. *Climate Dyn.,* **21**, 559–571.

Suzuki, R., S. K. Behera, S. Iizuka, and T. Yamagata, 2004: Indian Ocean subtropical dipole simulated using a coupled general circulation model. *J. Geophys. Res.,* **109**, C09001, doi: 10.1029/2003JC001974.

Thompson, D. W. J., and S. Solomon, 2002: Interpretation of Recent Southern Hemisphere Climate Change. *Science,* **296**, 895–899.

Torrence, C., and G. P. Compo, 1998: A practical guide to wavelet analysis. *Bull. Amer. Meteor. Soc.,* **79,** 61–78.

Venegas, S. A., L. A. Mysak, and D. N. Straub, 1997: Atmosphere–Ocean coupled variability in the South Atlantic. *J. Climate,* **10**, 2904–2920.

Venegas, S. A., L. A. Mysak, and D. N. Straub, 1998: An interdecadal climate cycle in the South Atlantic and its links to other ocean basins. *J. Geophys. Res.*, **103**, 24723–24736.

Wallace, C. S., and Q. R. Jiang, 1990: Spatial patterns of atmosphere–ocean interaction in the northern winter. *J. Climate,* **3**, 990–998.

Wallace, J. M., C. Smith, and C. S. Bretherton, 1992: Singular value decomposition of wintertime sea surface temperature and 500-mb height anomalies. *J. Climate,* **5**, 561–576.